WELDING RESEARCH

SUPPLEMENT TO THE *WELDING JOURNAL*, DECEMBER 1996
**Sponsored by the American Welding Society and the Welding Research Council**

# A Study on the Influence of Reflected Arc Light on Vision Sensors for Welding Automation

*Proposed model for predicting surface reflection seems to match well with experimental data*

**BY C. W. LEE AND S. J. NA**

ABSTRACT. Vision sensors using optical triangulation have been widely used for automatic welding systems in various ways. Their reliability is, however, seriously influenced by the arc light reflected from the base metal surface. In this study, the reliability of vision sensors was analyzed for the variation of the arc noise by considering the reflectance of the base metal surface. The property of the surface reflection of the base metal was modeled using the bidirectional reflectance-distribution function (BRDF), and then the intensity variation of the reflected arc was formulated for various configurations of the torch, base metal and sensor. The experimental data of the arc light reflection were obtained for two materials, mild steel and stainless steel, each having different surface reflection characteristics. It was found that the results calculated from the proposed model were in good agreement with the experimental data.

## Introduction

Gas metal arc welding is a common method for joining assemblies composed of thin sheet metal. With the low manual productivity resulting from the harsh environments and extreme physical demands, gas metal arc welding is considered a prime candidate for the application of industrial robots or mechanized equipment. The use of conventional robots in sheet metal arc welding is restricted by the difficulty of maintaining accurate fit-up and fixturing. Dimensional variations are introduced by pressing tools, fixtures and thermal distortions during welding. Therefore, it is necessary to introduce automatic tracking equipment to follow the actual path of the welding line.

Recently, many types of weld joint tracking sensors have been developed for improving the flexibility of arc welding robot applications. Among them, the active vision sensor, which utilizes a CCD camera, laser beam and computer, is effectively applicable to tracking the weld line of sheet metal joints without weaving due to its high resolution. The active vision sensor based on optical triangulation is classified into two types according to the beam characteristics: structured beam or scanning beam (Ref. 1). Although the vision sensor with structured light is largely influenced by arc noise and the preprocessing time of the image is long, it is widely used because it is relatively cheap and has a simple structure (Refs. 2–8). In spite of the complex structure and high price, the application of the vision sensor with the scanning beam increases steadily, because the effect of arc noise is low and the preprocessing time of the image is relatively short (Refs. 9–11).

Since the 1980s, much research has been conducted to apply vision sensor technology to welding automation. Until now, however, the resolution and the field of view were mainly considered in the design of the vision sensor, while the sensor reliability was only rarely investigated. Lenef, *et al.*, measured the arc spectrum to find the wavelength range of diode lasers, which would minimize the arc effect (Ref. 12). In their experiments, the base metal shape was neglected and diffuse reflection was assumed for the base metal surface. Nakata, *et al.*, studied the optimal configuration of optical components by varying the position and resolution of the camera and light source, and the camera exposure, etc. (Ref. 13). The results were, however, limited in the

**KEY WORDS**

Vision Sensor
Welding Automation
Specular Reflection
Diffuse Reflection
Torrance-Sparrow Model
Point Light Source
Arc Light
Laser Beam

*C. W. LEE is a Ph.D. candidate, Purdue University, Lafayette, Ind. S. J. NA is a Professor, Department of Mechanical Engineering, Korea Advanced Institute of Science and Technology, Taejon, Korea.*

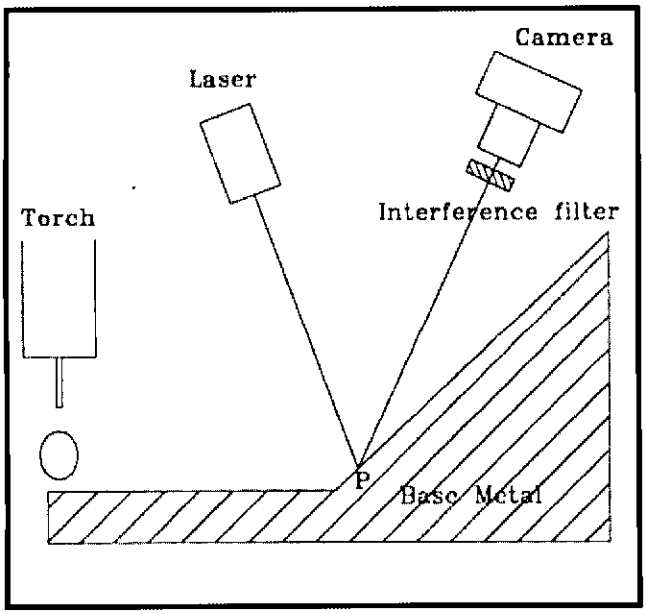


*Fig. 1 — Schematic diagram of welding system with vision sensor.*

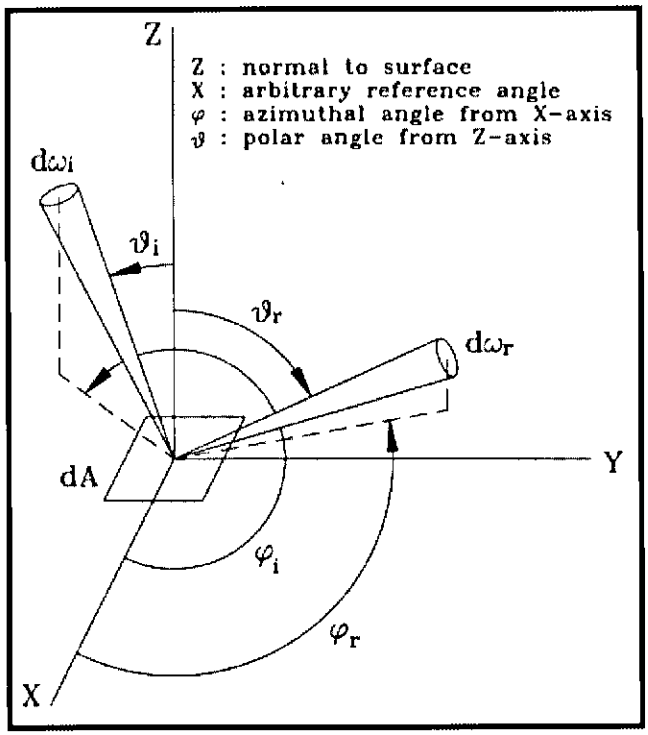


*Fig. 2 — Local geometry of arc reflection model.*

application, because the arc light was neglected and there was a lack of theoretical understanding to analyze experimental results. Nakata, *et al.*, also found that the effects of arc noise on the He-Ne laser decreased with the decreasing full width at half-maximum (FWHM) of the band pass filter (Ref. 14).

The important parameters influencing the vision sensor as the noise in arc welding are the arc light and spatter. Spatter is produced largely in gas metal arc welding with $CO_2$ shielding but emits mainly in the infrared range with a wavelength greater than 1.0 μm, due to its relatively low temperature (Ref. 7). Therefore, the arc light that is reflected from the base metal surface is considered to possess a dominant influence on the reliability of vision sensors, and consequently its effect has to be minimized by an appropriate geometrical configuration and the moving path of the sensor.

In this study, to improve the reliability of vision sensors for arc welding, the effect of the arc light was investigated as to the geometrical configuration of the sensor and welding arc, where various reflection properties of the base metal surface were considered. The base metal reflection was modeled in a two-dimensional domain, and the intensity of the arc image was formulated by assuming the arc light as a point light source. Various experiments were carried out to verify the validity of the proposed model.

## Theoretical Formulation

Figure 1 shows the typical configuration of an automatic welding system with a visual joint tracking sensor. The laser beam is reflected from the base metal surface in front of the welding arc, and the image pattern captured by the CCD camera is used to determine the weld joint shape. The interference filter located before the camera allows only the light with a wavelength range near that of the laser beam to pass through. At the same time, the arc light is also reflected from the base metal surface and captured by the CCD camera through the interference filter. The base metal shown in Fig. 1 has a slope so as to consider it as an inclined workpiece, such as the inside wall of a membrane-type LNG tank or the side panel of the container. In this study, only the arc noise reflected from the sensing area of the base metal surface, which is covered by the CCD camera and denoted by the point P in Fig. 1, was considered to formulate the magnitude of the arc light in accordance with the two-dimensional configuration of the arc, base metal and camera.

### Reflectance Model of Arc

The local coordinate system was adopted to represent the general reflectance characteristics, where an arbitrary direction was defined with (ϕ, θ) as in Fig. 2. The bidirectional reflectance distribution function (BRDF) $f_r$ is defined for the general expression of reflectance as follows (Ref. 15):

$$f_r(\theta_i, \phi_i, \theta_r, \phi_r) = \frac{dL_r(\theta_i, \phi_i, \theta_r, \phi_r, E}{dE_i(\theta_i, \phi_i)} \quad (1)$$

where $E_i(\theta_i, \phi_i)$ is the irradiance in the direction of $(\theta_i, \phi_i)$ and $L_r(\theta_i, \phi_i, \theta_r, \phi_r, E_i)$ the reflected radiance in the direction of $(\theta_r, \phi_r)$ caused by $E_i(\theta_i, \phi_i)$. $E_i$ is determined by the incident radiance $L_i$ and expressed as follows:

$$dE_i(\theta_i, \phi_i) = L_i(\theta_i, \phi_i) \cos \theta_i d\omega_i \quad (2)$$

where $d\omega_i = \sin \theta_i \, d\theta_i \, d\phi_i$ is the infinitesimal solid angle. By integrating Equation 2 in all directions on the hemispherical surface, $E_i$ is obtained as follows:

$$E_i = \int_{\omega} L_i \cos \theta_i d\omega_i \quad (3)$$

Similarly, $L_r$ can be obtained from Equations 1 and 2 as follows:

$$L_r = \int_{\omega} f_r L_i \cos \theta_i d\omega_i \quad (4)$$

Much research was conducted to establish the reflectance model. The research was either based on the numerical analysis because of its complexity, or it was too simple to obtain reliable results (Ref. 16). In this study, therefore, it was considered that the BRDF $f_r$ was composed of the fractions of the diffused reflection $f_{rd}$ and the specular reflection $f_{rs}$

$$f_r = f_{rd} + f_{rs} \quad (5)$$

The diffused reflection can be effectively expressed by the Lambertian model, which considers the uniform radiation in all directions. Therefore, the BRDF has a constant value a, which represents the level of the diffused reflection. The re-

flected radiance caused by the diffused reflection $L_d$ is derived by Lambert's cosine law as follows:

$$L_d = a\int_{\omega} L_i \cos\theta_i d\omega_i \tag{6}$$

It could be found that the reflected radiance caused by the diffused reflection is proportional to the incident energy.

The specular reflection is dependent on the surface of the workpiece, for which different models are available according to the ratio between the rms value of the surface roughness $R_q$ and the light wavelength $\lambda$ (Ref. 17).

**$R_q/\lambda > 1.5$**

Torrance, *et al.*, established a model based on the assumption that the rough surface was composed of specular elements arbitrarily arranged and showed that the Fresnel reflectance of a material has only a negligible effect on the BRDF (Refs. 18, 19). Neglecting the variation of the Fresnel reflectance in accordance with the angle change, the Torrance-Sparrow model can be expressed as follows (Ref. 18):

$$f_{rs} = b\left[\frac{G(\theta_i, \theta_r)}{\cos\theta_r}\right]\exp\left(-c^2\alpha^2\right)/\cos\theta_i \tag{7}$$

where $\alpha = (\theta_r - \theta_i)/2$ is the angle between the surface normal and the line equally dividing the incidence and reflection path, b the fraction of the specular reflection, and c the statistical distribution of the direction of specular elements. It was assumed that the surface normal, incidence path and reflection path were on the same plane ($\phi_i - \phi_r = 180$ deg, 0 deg). $G(\theta_i, \theta_r)$ was included to consider the effect of neighboring specular elements, and calculated by using the relationships listed in Table 1.

**Table 1 — Calculation formulas for $G(\theta_i,\theta_r)$ from Ref. 8**

| $0° \le \theta_i \le 45°$ | | $45° \le \theta_i \le 90°$ | |
|---|---|---|---|
| $\theta_r$ | $G(\theta_i,\theta_r)$ | $\theta_r$ | $G(\theta_i,\theta_r)$ |
| | | $90° \le \theta_r \le -\theta_i$ | Eq. A[a] |
| $-90° < \theta_r < \frac{\theta_i - 180°}{3}$ | Eq. A[a] | $-\theta_i \le \theta_r \le 3\theta_i - 180°$ | Eq. (a)* with $\theta_i,\theta_r$ interchanged |
| $\frac{\theta_i - 180°}{3} \le \theta_r \le \frac{\theta_i + 180°}{3}$ | 1 | | |
| $\frac{\theta_i + 180°}{3} \le \theta_r \le 90°$ | Eq. A[a] | $3\theta_i - 180° \le \theta_r \le \frac{\theta_i + 180}{3}$ | 1 |
| | | $\frac{\theta_i + 180°}{3} \le \theta_r \le 90°$ | Eq. A[a] |

a Equation A.

$$G(\theta_i,\theta_r) = 1 - \frac{[1 - (1 - A^2)^{1/2}]}{A}$$

$$A = \frac{\sin^2\theta_r - \cos^2[(\theta_r - \theta_i)/2]}{\cos^2[(\theta_i + \theta_i)/2] - \cos[\theta_r - \theta_i]\sin^2\theta_r}$$

**$R_q/\lambda \ll 1$**

For $\phi_i - \phi_r = 180$ deg, or 0 deg, the specular reflection has the same property as on the mirror and is modeled as follows:

$$f_{rs} = \frac{b\delta(\theta_i - \theta_r)}{(\sin\theta_r \cos\theta_r)} \tag{8}$$

where $\delta(\theta_i - \theta_r)$ is a function that satisfies the following:

$$\delta(\theta_i - \theta_r) = 1 \text{ for } \theta_i = \theta_r$$
$$\delta(\theta_i - \theta_r) = 0 \text{ for } \theta_i \neq \theta_r$$

**$R_q/\lambda \cong 1$**

The formulation of the specular reflectance is very complex and can be performed only by applying the physical model using the wave optics. However, it is known that the Torrance-Sparrow model can accurately predict the specular reflectance in this case, if no peak values occur. Furthermore, this case is encountered only rarely in applications of a vision-aided welding system, and thus was not formulated in this study.

**Arc Noise Model**

The energy spectrum radiated from the welding arc is composed of characteristic spectral lines of the plasma elements and ions and the black body emission (Refs. 14, 20, 21). The position and intensity of the characteristic spectral lines are known to be strongly influenced by the welding condition, base metal and shielding gas, while the black body emis-

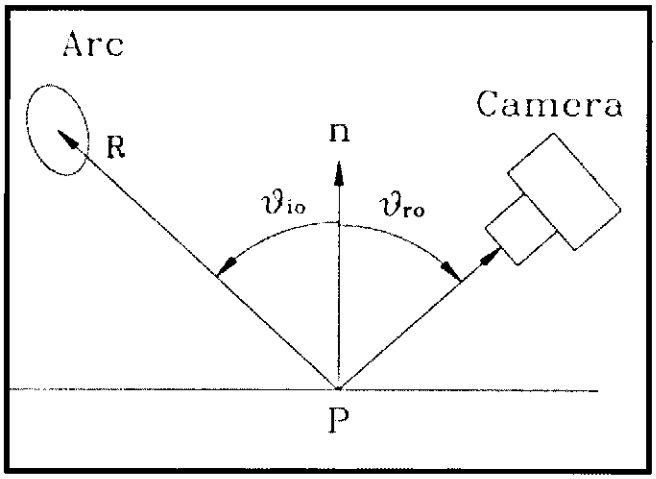


*Fig. 3 — Geometry of arc reflectance model.*

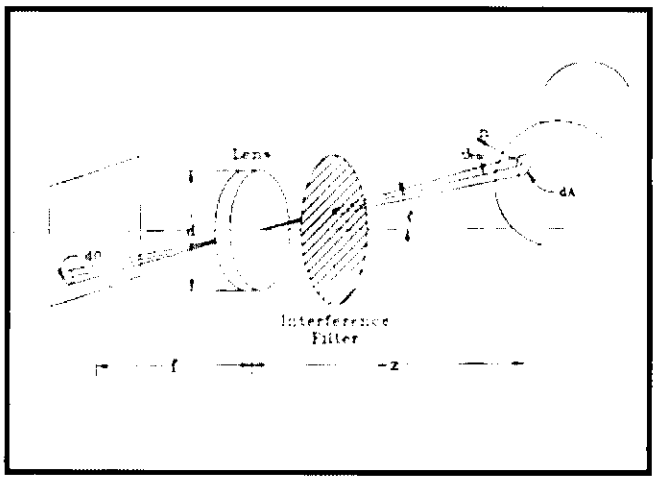


*Fig. 4 — Image forming system.*

**Table 2 — Specimens for Experiments**

| | Mild Steel | SUS304 |
|---|---|---|
| $R_a$(μm) | 1.44 | 0.16 |
| $R_q/\lambda$ | 2.1 | 0.23 |
| Processing | hot rolled | cold rolled |

**Table 3 — Conditions for Arc Noise Experiment**

| | Fig. 9 | Fig. 10 | Fig. 11 | Fig. 12 | Fig. 13 | Fig. 14 |
|---|---|---|---|---|---|---|
| Specimen | Mild Steel | Mild Steel | Stainless Steel | Mild Steel | Mild Steel | Stainless Steel |
| Welding Current (A) | GMAW 115 | GTAW 120 | GTAW 100 | GMAW 115 | GTAW 120 | GTAW 100 |
| Welding speed (mm/s) | 9 | 0 | 0 | 9 | 0 | 0 |
| R(mm) | | | | 72 | 62.5 | 50<br>80 |
| $\theta_{io}$(°) | 63 | 55 | 70 | | | |
| $\theta_{ro}$(°) | 55 | 35 | 20 | | | |
| $\theta_{so}$(°) | 118 | 90 | 90 | 125 | 90 | 90 |

sion can be expressed by Planck's law.

In Fig. 3, R is the distance between the arc center and base metal, $\theta_{io}$ the nominal angle of incidence between the surface normal and the line connecting the arc center and base metal, and $\theta_{ro}$ the nominal angle of reflection between the surface normal and the line connecting the camera lens center and base metal. The subscript o was added to denote that the angle is a nominal value. In this study, the arc center was assumed to be the hottest point in the arc. For the configuration of Fig. 3, if the effective area of the arc ($A_{eff}$) is negligibly small compared to the square of the distance between the arc and base metal ($R^2$), namely, $A_{eff} / R^2 \ll 1$, the irradiance $E_i(\lambda)$ can be modeled by assuming the arc as a point light source as follows:

$$E_i(\lambda) = I_\lambda(\lambda)\frac{\cos\theta_{io}}{R^2} \quad (9)$$

where $I_\lambda(\lambda)$ means the spectral radiant intensity of the arc (W/(sr Å)), which was assumed to be constant in this study. The radiance of the reflected arc $L_r(\lambda)$ is derived in a similar way as follows:

$$L_r(\lambda) = f_r(\theta_{io}, \theta_{ro}) \times I_\lambda(\lambda)\frac{\cos(\theta_{io})}{R^2} \quad (10)$$

In the vision-aided welding system, the distance from the welding arc to the sensing area of the base metal is normally greater than 2 cm (0.8 in.), while the effective area of the arc with the temperature higher than 10,000 K is approximately 0.5 cm². The isotherm of 10,000 K is frequently regarded as the boundary of welding arc, because severe deviations from LTE (local thermodynamic equilibrium) are likely for temperatures below 10,000 K (Ref. 22). Therefore, the assumption of $A_{eff} / R^2 \ll 1$ can be successfully adopted in this study.

### Image Model

The arc light reflected from the base metal surface is filtrated through the interference filter, condensed through the lens, and finally captured by the CCD camera to produce an image — Fig. 4. The relationship between the spectral radiance $L_r(\lambda)$ caused by the reflection on a surface point and the corresponding irradiance E on the image plane is modeled by considering the pass band of the interference filter as follows (Refs. 12, 16):

$$E(\lambda_c) = \left[\frac{\pi}{4}\cos^4\zeta / (f/d)^2\right] \int_0^\infty L_r(\lambda) F_G(\lambda - \lambda_c)\, d\lambda \quad (11)$$

where $\lambda_c$ is the center wavelength of the filter, $\zeta$ the angle between the optical axis and the line connecting the lens center and reflection point on the base metal, and f/d the camera F number. The term caused by the change of $\zeta$ was neglected, because the sensing area of the laser sensor was very small, which revealed that E was in a direct proportion to the radiance of the filtered arc light. $F_G(\lambda)$ is the spectral response of the interference filter and can be expressed in the Gaussian distribution function as follows:

$$F_G(\lambda) = t_r \exp\left(-\lambda^2 / 2\sigma^2\right) \quad (12)$$

where $\sigma = B_w/(2(2\ln 2)^{1/2})$ $t_r$ the peak transmittance and $B_w$ the FWHM of the filter.

The image sensor converts the irradiance E into the gray level $G_I$, which is expressed as follows:

$$G_I = pE^\gamma \quad (13)$$

where p is the proportional constant and $\gamma$ the $\gamma$ characteristic that is normally 1 for measurements, which results in a proportional relationship between $G_I$ and E.

### Gray Level of Arc Noise

The gray level of the arc reflected from the base metal surface $G_a(\lambda_c)$ is obtained by combining Equations 11, 12 and 14 as follows:

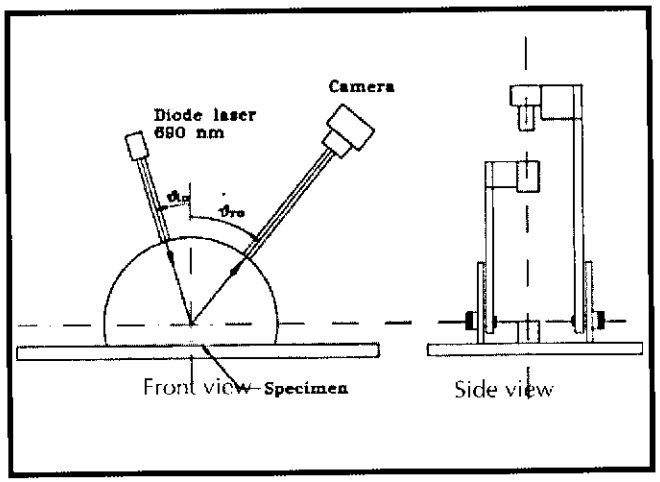


*Fig. 5 — Apparatus for measuring laser reflection.*

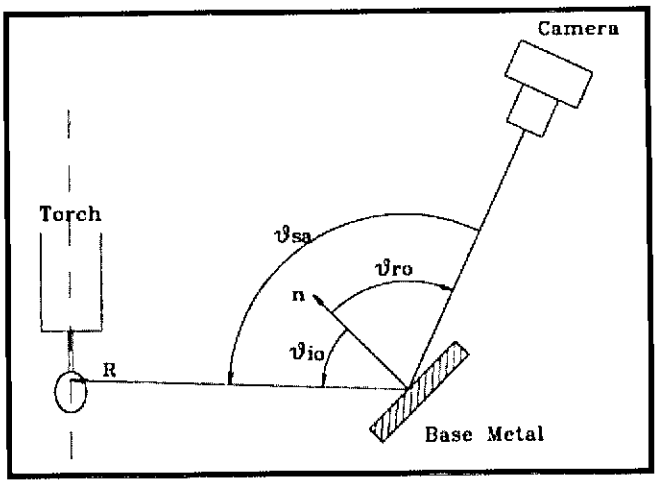


*Fig. 6 — Configuration of arc reflection experiments.*

$$G_d(\lambda_c) = K\left[H(\lambda_c) f_r(\theta_{io}, \theta_{ro}) \frac{\cos\theta_{io}}{R^2}\right]^{\gamma} \quad (14)$$

where K is a constant, $H(\lambda_c)$ the radiant intensity of the arc filtered through the interference filter with the center wavelength of $\lambda_c$ and the peak transmittance of 1, which can be expressed as follows:

$$K = p\left\{t_r\left[\frac{\pi}{4}\cos^4\zeta / (f/d)^2\right]\right\} \quad (15a)$$

$$H(\lambda_c) = \frac{1}{t_r}\int_0^{\infty} I_\lambda(\lambda) F_G(\lambda - \lambda_c)\, d\lambda \quad (15b)$$

#### Reflectance Model of Laser

For calculating the BRDF from the reflectance model of arc, three BRDF parameters a, b and c should be determined through the experiments. A diode laser with a wavelength of 690 nm, which has been widely used for active vision sensors, was applied to determine these constants, because they should be most fit to the reflectance model of the arc light that passed through the interference filter of the vision sensors.

In laser sensors, the laser beam can be considered as a parallel light source because a large focal length of the lens is generally preferred to enlarge the depth of field. For the parallel light source, the reflectance model can be derived as follows:

$$L_r = f_r(\theta_{io}, \theta_{ro}) E_o \cos\theta_{io} \quad (16)$$

where $E_o$ is the irradiance of the parallel light perpendicular to the reflecting surface and $\theta_{io}$, $\theta_{ro}$ are the nominal angles of incidence and reflection, respectively. Here, the subscript o was added again to denote a nominal value. The gray level of the reflected laser beam $G_l(\lambda_c)$ can be then derived as follows:

$$G_l(\lambda_c) = K\left[E_o f_r(\theta_{io}, \theta_{ro}) \cos\theta_{io}\right]^{\gamma} \quad (17)$$

## Experiments

Experiments were carried out first to determine the BRDF parameters, and second to verify the validity of the proposed reflectance model of the arc.

#### Experiments for BRDF Parameters

The schematic diagram of the experimental apparatus is shown in Fig. 5. The diode laser with a wavelength of 690 nm was used to supply the parallel light, while the image was captured by a CCD camera with a $\gamma$ characteristic value of 0.45. A band-pass filter, which had the same center wavelength as the laser and a FWHM of 11 nm, was placed in front of the camera to consider the actual configuration of practical sensors. The specimens were prepared from the hot-rolled mild steel and 304 type stainless steel, whose surface roughness and $R_q/\lambda$ are given in Table 2, because the reflectance model was derived according to the ratio between the surface roughness and wavelength.

#### Experiments for Arc Noise Model

The experimental apparatus is schematically shown in Fig. 6, where the components such as the camera and band-pass filter are of the same characteristics as in Fig. 5. The magnitude of the gray level of the reflected arc light was obtained by averaging 20 values measured every 0.2 s. To verify the validity of the assumption of considering the arc light as a point light source, the reflected arc light was first measured for various R values under the fixed angles of incidence and reflection, and second for various angles of reflection under the fixed R and angle of separation ($\theta_{so}$). In this case, the angle of incidence was determined by subtracting the angle of reflection from the fixed $\theta_{so}$ value. In experiments, the distance between the arc and reflection area was varied from 45 mm (1.8 in.) to larger values, because too small R values would enormously decrease the validity of the assumption of a point light source. For thick section welding, which almost always involves welding in a groove, however, a 45-mm distance between the arc and reflection area is too great. Therefore, the results of this

**Table 4 — Results of Nonlinear Regression for Mild Steel Using Gauss-Newton Method**

| | b/a | $c^2$ |
|---|---|---|
| Obtained value | 1.87 | 51.4 |
| Asymptotic standard error | 1.80 | 19.8 |

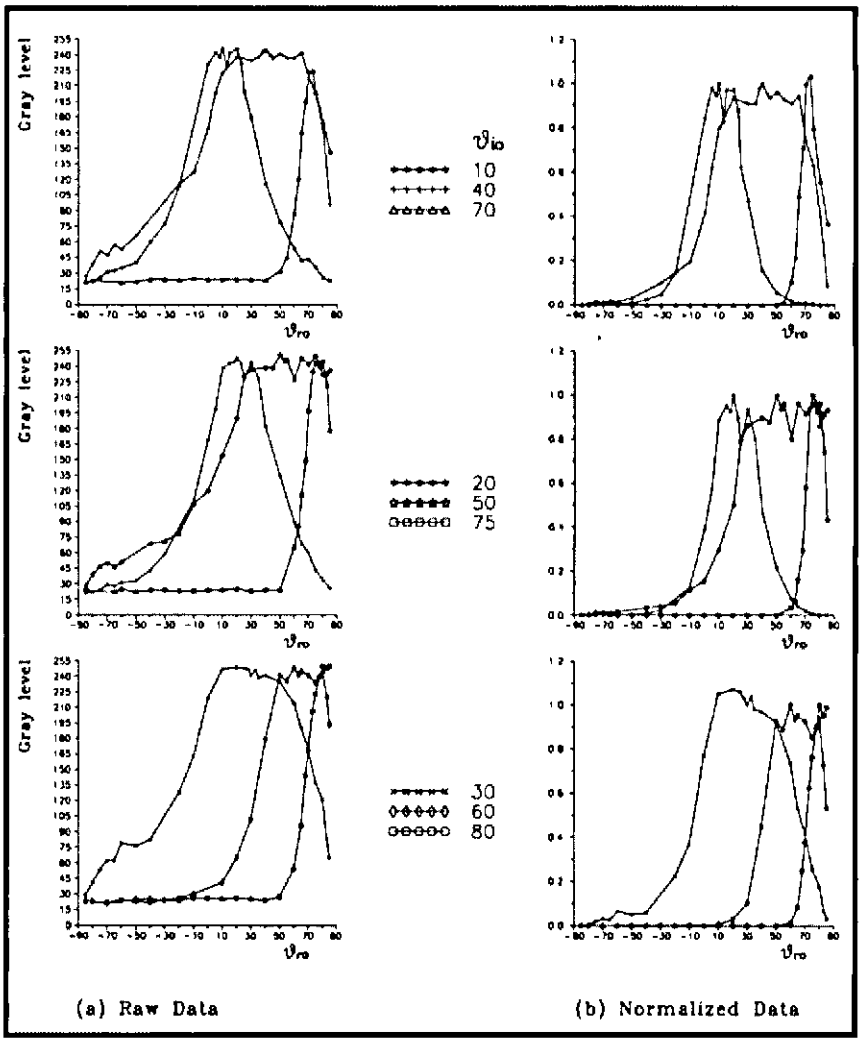


*Fig. 7 — BRDF distribution of hot-rolled mild steel.*

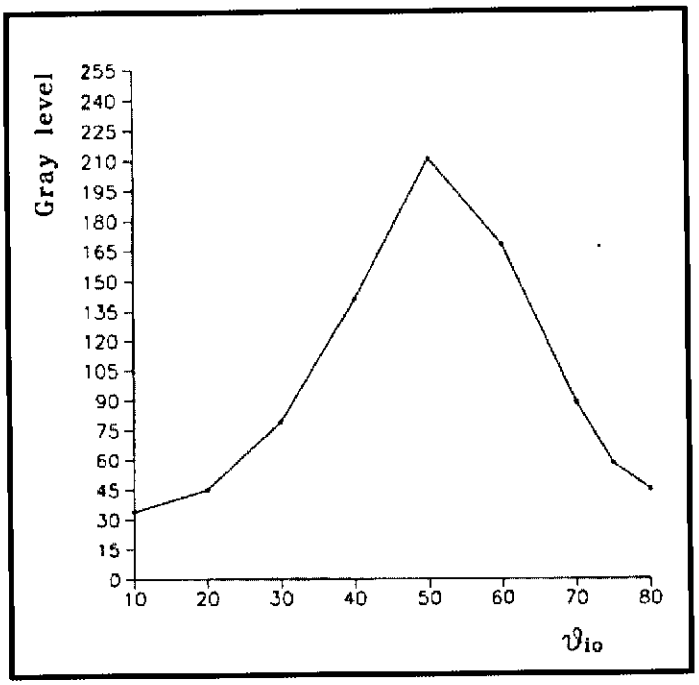


*Fig. 8 — Image intensity distribution of hot-rolled mild steel for $\theta_{ro}$ = 50 deg.*

paper can be applied to thin-section welding on an inclined workpiece such as the inside wall of the membrane type LNG tank or the side panel of the container. For welding in a groove of thick plates, the arc noise model should be expanded to include the spatial distribution of the welding arc.

In calculations, the arc position was assumed to be 1 mm (0.04 in.) under the electrode tip in GTA (gas tungsten arc) welding, and 3 mm (0.12 in.) over the specimen surface in GMA (gas metal arc) welding, for which the arc length was assumed to be 4 mm (0.16 in.). This was due to the presumption that the welding arc had its maximum temperature at 1 mm under the electrode tip. Table 3 shows the welding conditions chosen for measuring the arc noise.

## Results and Discussion

Figure 7 shows the measured gray level of the laser light reflected from the hot-rolled mild steel plate, which was considered to be appropriate for applying the Torrance-Sparrow model. The angle of reflection was varied in a wide range, while the angle of incidence was fixed at the values between 10 and 80 deg. Figure 7A shows the gray level values obtained directly from the CCD camera. They were then normalized with regard to the gray level obtained under the condition that the angle of reflection was the same as the angle of incidence, and the results are shown in Fig. 7B. As expected from the Torrance-Sparrow model, there exists a specular lobe, and the mirror surface reflection can be assumed for large angles of incidence.

Figure 8 shows the gray levels of the reflected laser light measured at 9 different $\theta_{io}$ values under the fixed $\theta_{ro}$ = 50 deg. The results were then normalized with regard to the case of $\theta_{io} = \theta_{ro}$= 50 deg. These normalized data were then used as the reference values to normalize the corresponding data in Fig. 7B of the same $\theta_{io} = \theta_{ro}$= 50 deg, which were then used to substitute the Lambertian model and Torrance-Sparrow model into Equation 5. The resultant equation was then used for the nonlinear regression with the Gauss-Newton method to obtain three BRDF parameters, and the resultant a, b and c values are shown in Table 4.

The parameter b for the case of Rq/λ « 1 could not be determined, because the peak gray level of the laser light reflected from the stainless steel plate was always over the dynamic response range of the CCD camera.

Figure 9 shows the gray level of the arc in GMAW reflected from the hot-rolled mild steel plate with respect to the distance between the arc and reflection area. Figure 10 shows that in GTAW. The data in Figs. 9B and 10B were determined by normalizing the gray levels of

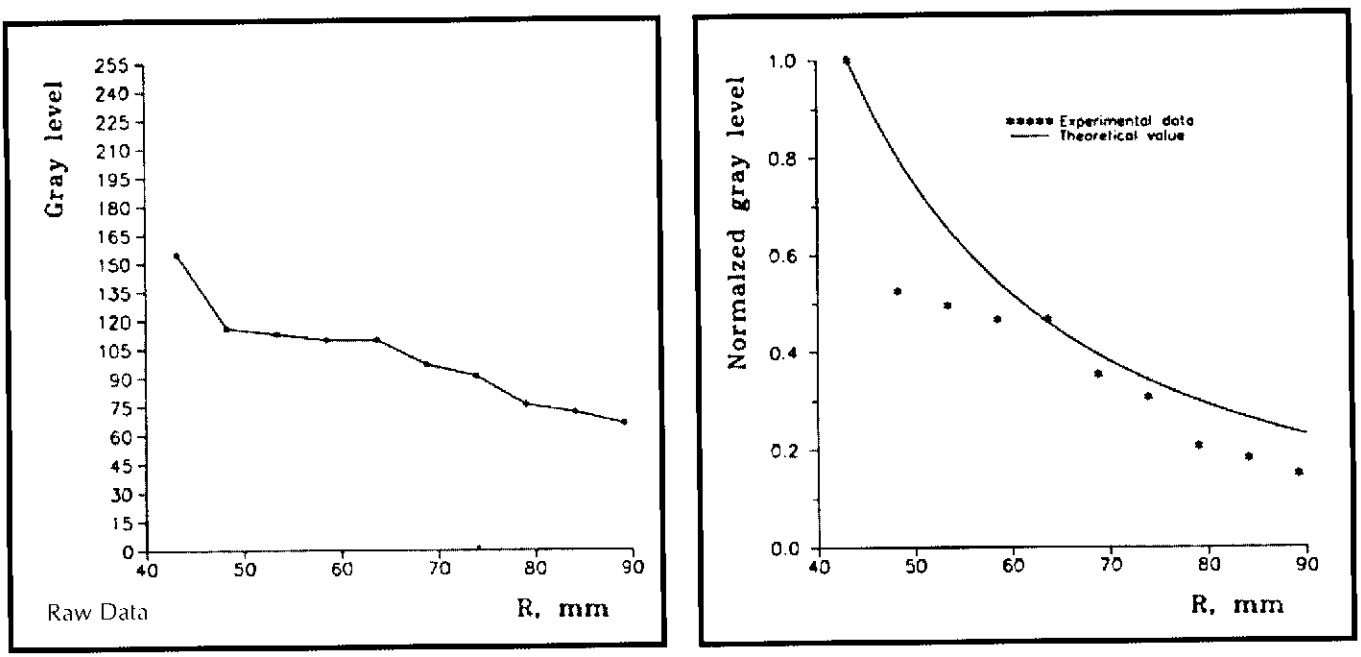


*Fig. 9 — Intensity of GMAW arc reflected from hot-rolled mild steel with varying R.*

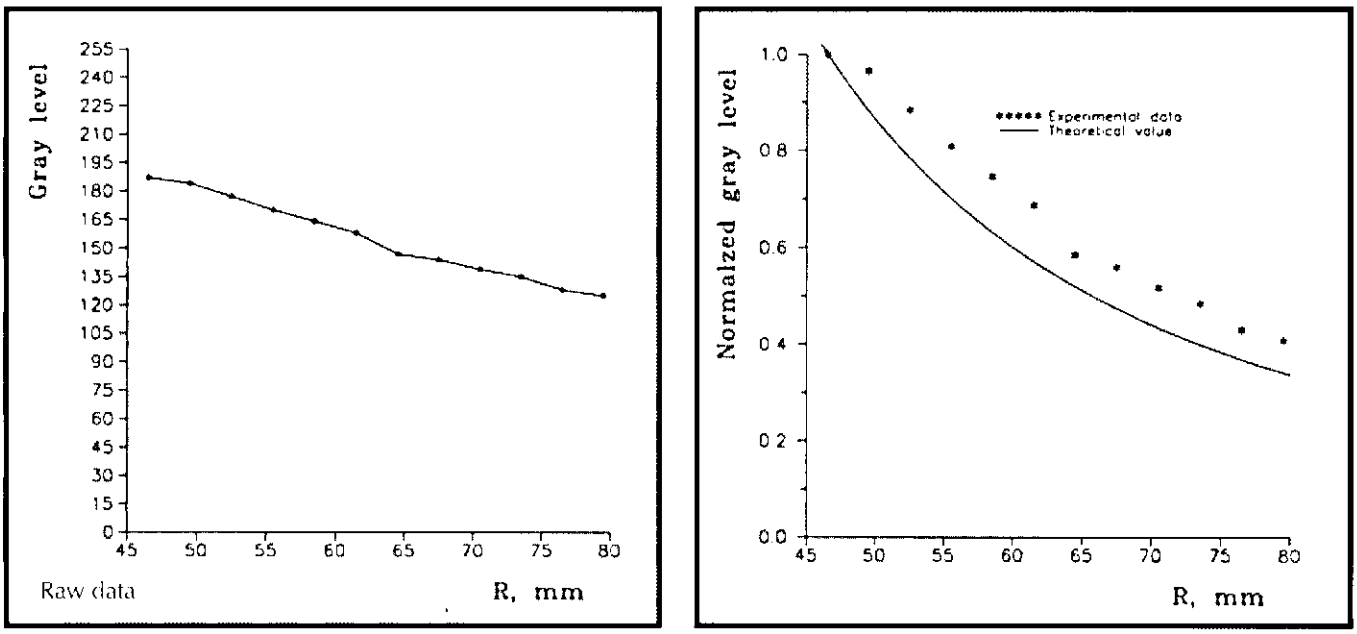


*Fig. 10 — Intensity of GTAW arc reflected from hot-rolled mild steel with varying R.*

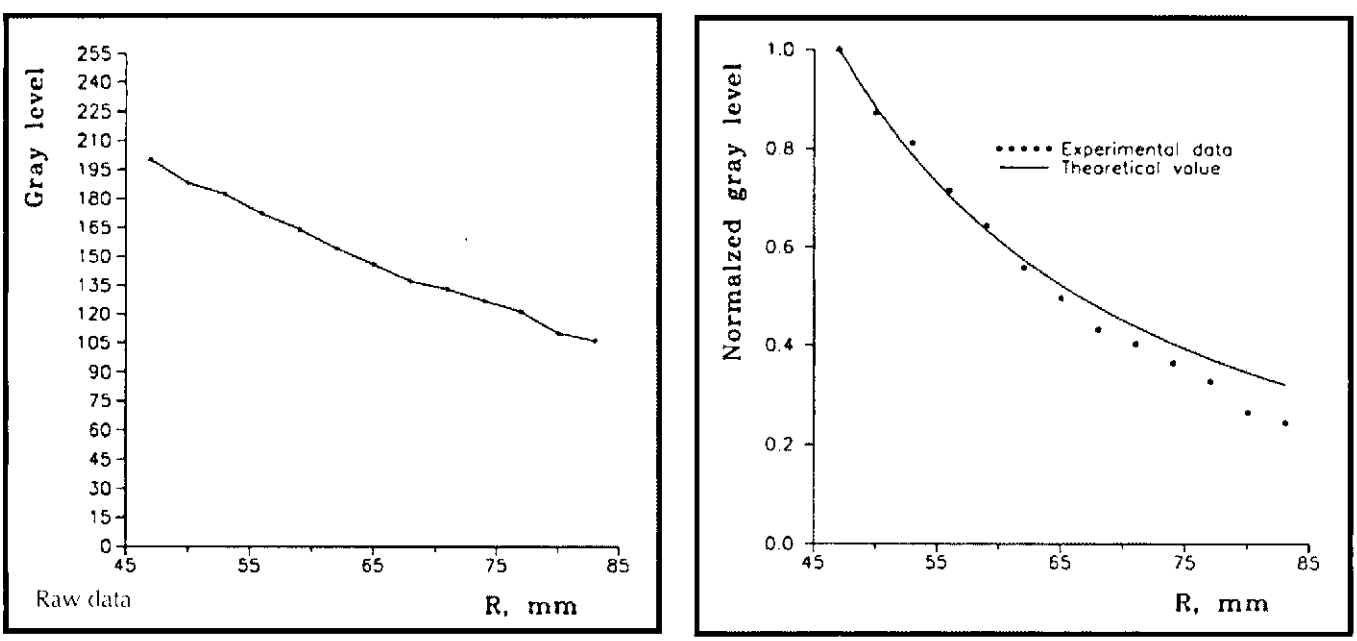


*Fig. 11 — Intensity of GTAW arc reflected from stainless steel with varying R.*

the CCD camera with regard to the value at minimum R after compensating them with the γ characteristic of the CCD camera. That is, (measured gray level)$^{1/\gamma}$ was divided by (maximum gray level)$^{1/\gamma}$ to give the normalized data of the gray level, which would then show the theoretical relationship that the normalized gray level is reversely proportional to $R^2$. By comparing the results in Figs. 9B and 10B, it can be shown that the arc in GTAW corresponds to the theoretical value better than the arc in GMAW. This is probably due to the fact that the arc in GTAW is generally smaller than that in GMAW, and consequently, the former would act as a point light source more suitably than the latter.

The experimental results obtained with 304 type stainless steel plates are shown with respect to the distance between the arc and workpiece — Fig. 11. The normalized values of the measured gray levels were in good agreement with the theoretical values calculated from the simple relationship of $1/R^2$, which had a magnitude of 1 at R = 45 mm. From these experimental and theoretical results, it might be concluded that the welding arc can be assumed as a point light source for establishing the reflectance model of the arc noise in vision sensors, especially for the arc in GTAW and for a long distance between the arc and reflection surface.

Figure 12 shows the experimental results for the arc in GMAW reflected from the hot-rolled mild steel surface. Figure 13 shows the results from GTAW. Experiments were carried out for various angles of reflection, while R and $\theta_{cs}$ were fixed at 72 mm (2.8 in.) and 125 deg for Fig. 12, and 62.5 mm (2.5 in.) and 90 deg for Fig. 13. The specular characteristic was considerably high around the angle of reflection of 62.5 deg in Fig. 12 and 45

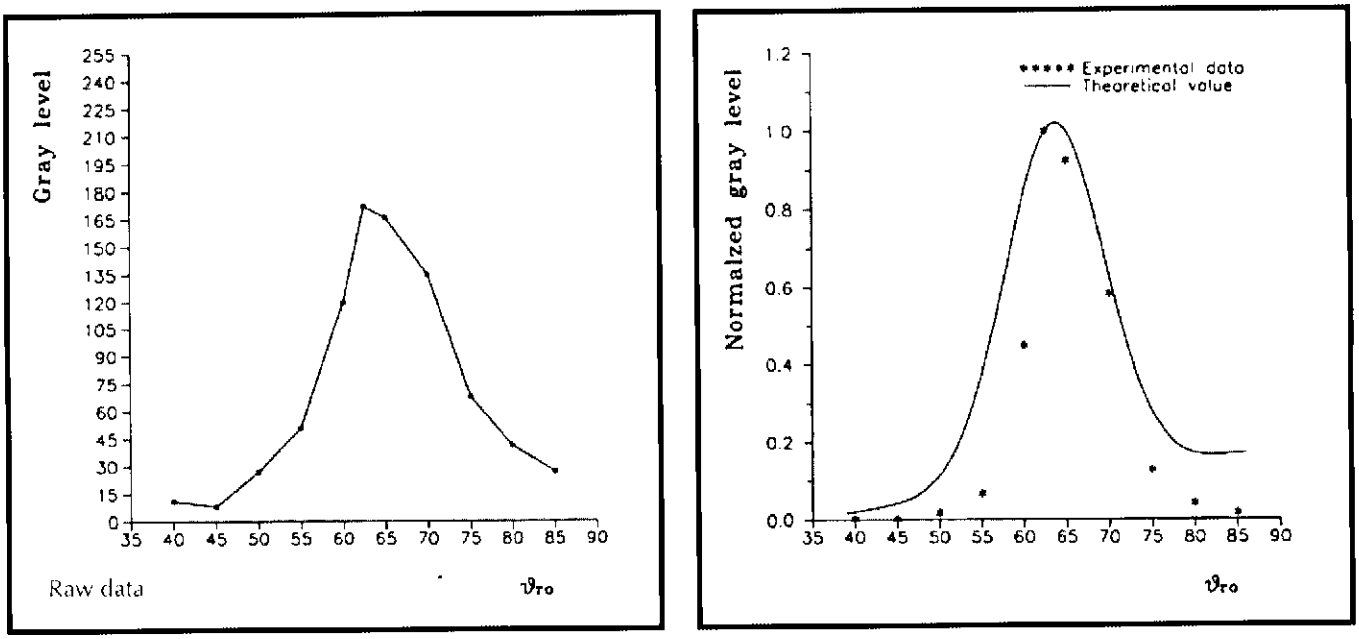


*Fig. 12 — Intensity of GMAW arc reflected from hot-rolled mild steel with varying angle of reflection.*

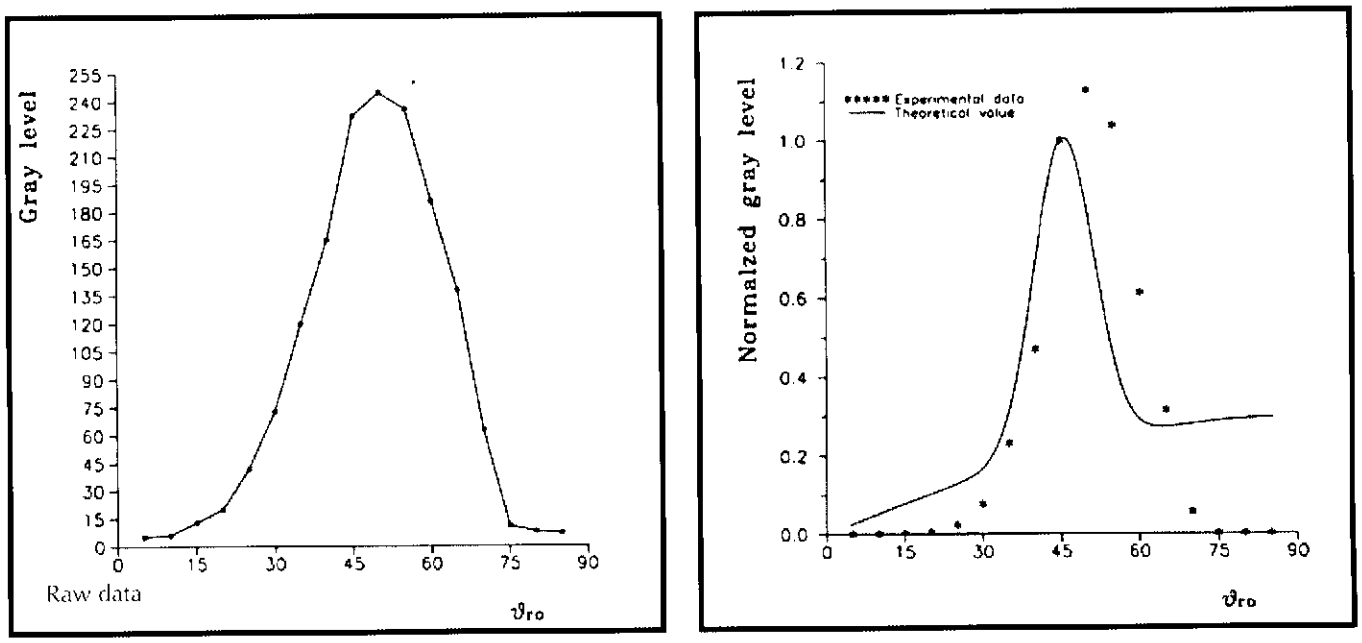


*Fig. 13 — Intensity of GTAW arc reflected from hot-rolled mild steel with varying angle of reflection.*

deg in Fig. 13, which were the cases of $\theta_{ic} = \theta_{ic}$. These high gray levels of the reflected arc could cause a substantial noise in the image data of vision sensors. By comparing the normalized data of the measured gray level with the simulated values, it was revealed that the Torrance-Sparrow model can fairly well predict the reflectance behavior of the welding arc, and therefore can be effectively used for the design of the visual joint tracking sensor of the arc welding process.

Figure 14 shows the gray level of the arc in GTAW reflected from the stainless steel plate. The data were measured for the fixed $\theta_{ic}$ value of 90 deg and two different R values of 60 and 80 mm. It could be revealed that for a shorter distance between the welding arc and base metal, high gray levels were measured over a wider range of $\theta_{rc}$. This is probably due to the fact that the welding arc from a short distance would act as a somewhat extended light source rather than a point light source. In case of the similar angles of incidence and reflection, high gray levels of the reflected arc would considerably influence the performance of vision sensors.

## Conclusions

Vision sensors using optical triangulation have been widely used for automatic joint tracking in the arc welding process. The reliability of the vision sensor would be considerably influenced by the arc light reflected from the base metal surface. In this study, therefore, the re-

flectance model of the welding arc was derived to estimate the arc noise for various configurations of the sensor, base metal and welding arc. Various experiments were carried out first to determine the BRDF parameters of the model, and second to verify the validity of the proposed model. Experimental results of the gray level of the reflected arc agreed fairly well with the calculated ones, which were reversely proportional to the square of the distance between the welding arc and reflecting area. It was revealed that the arc light can be assumed as a point light source in the reflectance model for the distance between the welding arc and base metal greater than about 45 mm. It was also found that the Torrance-Sparrow model can be effectively adopted for the arc reflection on the hot-rolled mild steel plate. Experimental and calculated results showed that considerably high gray levels of the reflected arc may be captured by the vision sensor, which has then a considerable influence on the performance of sensors.

The proposed model and experimental results can be effectively used for the design of the configuration and moving path of vision sensors according to the base metal shape, which can then reduce the effect of arc noise on the vision sensor and consequently improve its reliability in automatic joint tracking of the arc welding process. To enlarge the usefulness of the proposed model, further work should be done about the finite size of the welding arc and also about the method to find the optimal configuration and moving path of vision sensors for minimizing the arc noise.

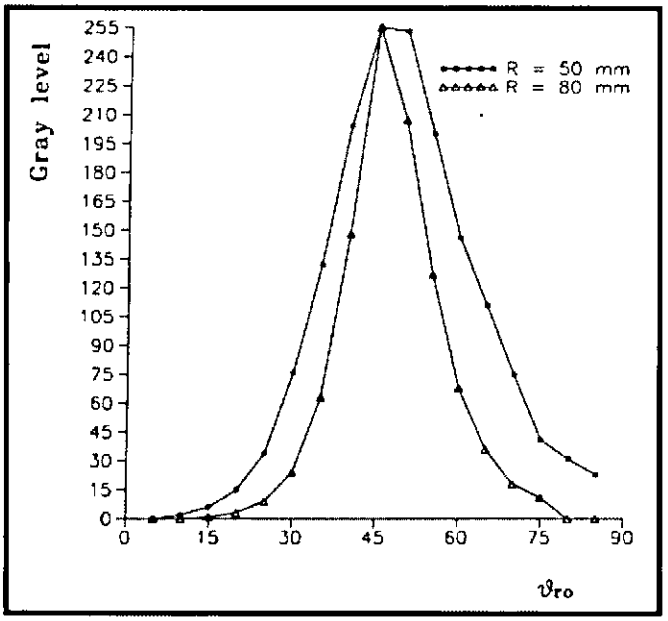


*Fig. 14 — Intensity of GTAW arc reflected from stainless steel with varying angle of reflection.*


*Acknowledgment*

This work has been partially supported by Kuk-Min Bank and YIENT Co., Ltd., Korea.


*References*


1. Lee, C. W., and Na, S. J. 1993. Vision sensor for welding automation. *Journal of the Korean Welding Society* 11(3):10–21.

2. Clocksin, W. F., Bromley, J. S. E., Davey, P. G., Vidler, A. R., and Morgan, C. G. 1985. An implementation of model-based visual feedback for robot arc welding of thin sheet steel. *The International Journal of Robotics Research* 4(1): 13–26.

3. Richardson, R. W. 1986. Robotic weld joint tracking systems — theory and implementation methods. *Welding Journal* 65(11): 43–51.

4. Agapakis, J. E., Katz, J. M., Koifman, M., Epstein, G. N., Friedman, J. M., Eyring, D. O., and Rutishauser, H. J. 1986. Joint tracking and adaptive robotic welding using vision sensing of the weld joint geometry. *Welding Journal* 65 (11): 33–41.

5. Niepold, R., and Brummer, F. 1987. PASS — a visual sensor for seam tracking and on-line process parameter control in arc welding applications. *Robotic Welding*, IFS Ltd., pp. 129–140.

6. Beattie, R. J., Cheng, S. K., and Logue, P. S. 1988. The use of vision sensors in multipass welding applications. *Welding Journal* 67(11): 28–33.

7. Sin, J. S. 1991. A Study on Seam Tracking and Arc Data Monitoring System in Lap Joint, M. S. Thesis, Korea Advanced Institute of Science and Technology.

8. Huissoon, J. P., Strauss, D. L., and Stefaniuk, W. P. 1992. Dynamic seam tracking for weld process control. *Proceed. Int. Conf. on Computerization of Welding Information*, Orlando, Fla., pp. 226–239.

9. Oomen, G. L., and Verbeek, W. J. P. A. 1987. A real-time optical profile sensor for robot arc welding. *Robotic Welding*, IFS Ltd., pp. 117–128.

10. Bjorkelund, M. 1987. A true seam-tracker for arc welding. *Robotic Welding*, IFS Ltd., pp. 167–177.

11. Nitzan, D. 1988. Three-dimensional vision structure for robot applications. *IEEE Trans. on PAMI* 10(3): 291–309.

12. Lenef, L., and Gardner, C. S. 1985. Optical emissions from weld arcs and their effects on the performance of welding robot vision systems. *Applied Optics* 24(16): 2587–2595.

13. Nakata, S., Jie, H., Tsuruha, Y., Noguchi, N., and Kobashiri, T. 1988. Visual sensing system for in-process control of arc welding process. *Welding International* 2(12): 1086–1090.

14. Nakata, S., Jie, H., Tsuruha, Y., Kobashiri, T., and Makino, Y. 1989. Determination on geometrical arrangement of optical equipments and photographic parameters for construction of visual sensing system. *Quarterly Journal of the Japan Welding Society* 7(3): 358–362.

15. Nicodemus, F. E., Richmond, J.C., Hsia, J. J., Ginsberg, I. W., and Limperis, T. 1977. *Geometrical Considerations and Nomenclature for Reflectance*. NBS Monograph 160, National Bureau of Standards, Washington, D.C.

16. Horn, B. K. P. 1986. *Robot Vision*, MIT Press.

17. Nayar, S. K., Ikeuchi, K., and Kanade, T. 1990. Determining shape and reflectance of hybrid surfaces by photometric sampling. *IEEE Trans. on Robotics and Automation* 6(4): 418–431.

18. Torrance, K. E., and Sparrow, E. M. 1967. Theory for off-specular reflection from roughened surfaces. *Journal of the Optical Society of America* 57(9):1105–1114.

19. Torrance, K. E., and Sparrow, E. M. 1966. Off-specular peaks in the directional distribution of reflected thermal radiation. *Journal of Heat Transfer-Trans. of ASME(C)* 88(2): 223–230.

20. Inoue, K. 1981. Image processing for on-line detection of welding process (Rep. 3) improvement of image quality by incorporation of spectrum of arc. *Trans. of Japan Welding Research Institute* 10(1): 13–18.

21. Kim, E. W., Allemand, C., and Eagar, T. W. 1987. Visible light emissions during GTAW and its application to weld image improvement. *Welding Journal* 66(12): 369-s to 377-s.

22. Hsu, K. C., Etemadi, K., and Pfender, E. 1983. Study of the free-burning high intensity argon arc. *Journal of Applied Physics* 54(3): 1293–1301.